Available online at www.sciencedirect.com

SciVerse ScienceDirect

Scripta Materialia 69 (2013) 25–28

Scripta MATERIALIA

www.elsevier.com/locate/scriptamat

Anisotropic grain growth and crack propagation in eutectic microstructure under cyclic temperature annealing in flip-chip SnPb composite solder joints

Y.C. Liang,[a] H.W. Lin,[a] H.P. Chen,[b] C. Chen,[a,*] K.N. Tu[b] and Y.S. Lai[c]

[a] *Department of Materials Science and Engineering, National Chiao Tung University, Hsin-chu 30010, Taiwan, ROC*
[b] *Department of Materials Science and Engineering, University of California at Los Angeles, Los Angeles, CA 90095, USA*
[c] *Central Laboratories, Advanced Semiconductor Engineering Inc., Kao-hsiung 811, Taiwan, ROC*

Received 8 March 2013; revised 18 March 2013; accepted 18 March 2013
Available online 22 March 2013

The evolution of eutectic structure under temperature cycling tests (TCTs) in SnPb composite solder joints has been investigated. After 500 cycles of TCT, the Sn grains coarsened and developed anisotropic stripes close to the necking site in the solder joint because of stress-induced atomic migration. Then, cracks triggered by thermal stress were observed to propagate along the Sn stripe interfaces. After a prolonged 14,410 cycles of TCT, the cracks expanded across the entire solder joint and led to electrical open failure.

Keywords: Stress migration; Diffusion; Temperature cycling test; SnPb composite solder joint

For high-density electronic packaging, the application of flip-chip solder joints has been well received in the microelectronics industry [1]. High-lead (Pb) solders such as Sn5Pb95 [2–6] are presently granted immunity from the Restriction of Hazardous Substances (RoHS) requirements for their use in high-end flip-chip devices, especially in military applications. In flip-chip technology for consumer electronic products, organic substrates have replaced ceramic substrates due to the demand for less weight and low cost. However, the liquidus temperatures of high-Pb solders are over 300 °C which would damage organic substrates during reflow because of the low glass transition temperature. To overcome this difficulty, the composite solder approach was developed [7]. By using an eutectic Sn63Pb37 solder bump on the substrate side in combination with a high-Pb solder bump on the chip side, as illustrated in Figure 1a, a much lower reflow temperature (slightly over the melting point of the eutectic solder) can be used without damaging the organic substrates. During reflow, the Sn63Pb37 solder melts and dissolves some of the Sn5Pb95 solder to form a joint. As shown in Figure 1b, most of the eutectic phase remains on the substrate side in the solidified composite solder joint. No intermixing of the high-Pb and the eutectic occurs.

In the literature, several studies regarding the reliability issues of flip-chip SnPb composite solder joints have been reported [8–12]. Fatigue failure of flip-chip SnPb composite solder joints has been researched through various reliability tests [8]. Chang et al. investigated the intermixing of high-Pb solder and eutectic during reflow [9]. They found that the latter had a calyx shape and the height of the calyx-shape bump increased with reflow time. This group also reported that the intermetallic compound (IMC) Ni_3Sn_4 on the chip side converted into $(Cu,Ni)_6Sn_5$ after an extended aging time [10]. In addition, electromigration- and thermomigration-induced failure have been observed in SnPb composite solder joints [11,12].

Several investigations on stress-induced migration in Cu interconnects have been carried out [13–15]. In addition, stress has been found to induce Sn whisker issues in solder joints [16–18]. However, no study has addressed the phenomenon of stress-induced migration in flip-chip SnPb composite solder joints. We note also that satellites are subject to temperature cycles in space [19]. The way in which cyclic thermal stress-induced stress migration affects the reliability of solder joints requires

* Corresponding author. Tel.: +886 3 5731814; fax: +886 3 5724727; e-mail: chih@mail.nctu.edu.tw

1359-6462/$ - see front matter © 2013 Acta Materialia Inc. Published by Elsevier Ltd. All rights reserved.
http://dx.doi.org/10.1016/j.scriptamat.2013.03.018

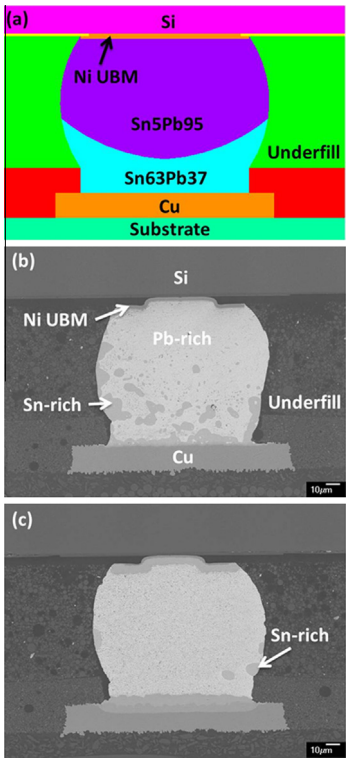

Figure 1. (a) Schematic diagram for the solder joint structure used in this study. (b) Cross-sectional SEM images showing the as-reflowed SnPb composite solder joint. (c) Cross-sectional SEM image for the solder bump after an isothermal annealing at 150 °C for 2160 h.

a systematic study. In this study, we investigate the evolution of microstructure in the composite solder joint under isothermal and temperature cycle annealing. The latter has caused open failures by stress-induced growth of anisotropic Sn grains and crack formation and propagation along the Sn/Pb interfaces over the entire composite solder joint.

The test vehicles were 27 mm × 27 mm × 1.39 mm flip-chip packages, which involve a 7.62 × 7.62 × 0.73 mm silicon chip interconnected to a 0.56 mm thick organic substrate by 720 solder joints. The pitch between adjacent solder joints was 270 μm. Beneath a 3 μm thick Ni under-bump-metallization (UBM), an electroplated solder of Sn5Pb95 was reflowed at 350 °C to form a spherical high-Pb solder bump with a diameter of 95 μm on the chip side. The substrate pad metallization featured the solder on pad (SOP) surface treatment, i.e. with printed Sn63Pb37 eutectic solder on the Cu pad surface. The high-Pb solder bump and the SOP were then reflowed at 240 °C to become SnPb composite solder joints as shown in Figure 1a and b.

To investigate the evolution of eutectic microstructure in flip-chip SnPb composite solder joints, the samples were subjected to either TCT or isothermal annealing. The TCT condition was between −55 and 125 °C for 100, 500, 1500, 2160, and 14410 cycles with each cycle period of 1 h. Isothermal annealing tests at 150 °C for 2160 h were also applied to fresh samples, providing a comparison of the thermo-mechanical characteristics of the different heat treatments. Figure 1(c) shows the microstructure change after the isothermal annealing at 150 °C for 2160 h. During isothermal annealing, some of the Sn-rich phase was consumed by reacting with the Ni UBM and the Cu metallization pad layer to form IMCs. The remaining Sn grains became circular and dramatically decreased in volume in the SnPb composite solder joint.

Cross-sections of the samples after the temperature cycling tests (TCTs) and the isothermal annealing test were mechanically polished, and the microstructure on the cross-sections was observed by scanning electron microscopy (SEM) using a microscope with a back-scattered electron image detector. Moreover, the composition of the solder joints and the IMCs was examined by energy dispersive spectroscopy. The IMC of Ni_3Sn_4 was formed at the interface of the Ni UBM and the high-Pb solder on the chip side, whereas Cu_6Sn_5 and Cu_3Sn were formed at the interface of the eutectic solder and the Cu metallization layer on the substrate side.

Under TCT, the formation of horizontally anisotropic Sn stripes in the composite solder joints was observed. Figure 2a shows the cross-section of the solder bump after 500 cycles of TCT. The grains of the Sn-rich phase coarsened along the horizontal direction and were laid at a similar position in height, before and after the thermal cycles. The position was at about one-third of the bump height from the Cu pad metallization layer, which was close to the necking site in the solder bump due to the pad opening defined by the solder mask at the substrate side. Moreover, the position is close to the interface between the high-Pb and the eutectic, because the height of the eutectic solder before joining to the high-Pb is defined by the solder mask. After 1500 cycles of TCT, as demonstrated in Figure 2c, the small Sn grains grew into a longer Sn stripe near the necking site in the solder bump.

Figure 2e illustrates the cross-section of the solder bump after 14410 cycles of TCT. The anisotropic growth of the Sn stripe appears to have grown across the entire solder bump. However, crack propagation along the horizontal Sn–Pb interfaces in the solder bump can be clearly observed after 14410 cycles of TCT.

To examine the crack propagation, a second cross-section across the horizontal Sn stripe interfaces polished by focused ion beam (FIB) rendered a better crack appearance. Using FIB, the cracks were clearly revealed without coverage by impurities during the mechanical polishing. Figure 2b, d and f represent the second cross-sections of the solder bumps polished by FIB after 500, 1500 and 14410 cycles of TCT, respectively. We note that these images have been rotated 90° with respect to those in Figure 2a, c and e. It can be seen that the cracks formed along the Sn–Pb interfaces in the as-fabricated state and expanded greatly along the stripe Sn–Pb interfaces after 14410 cycles of TCT.

During isothermal annealing, the Sn atoms diffused a distance of about 50 μm to react with UBMs to form IMCs, instead of forming Sn stripes as in TCT. Additionally, as illustrated in Figure 1c, no Sn stripes except circular Sn grains were observed in the solder bump. A literature search revealed that the present finding of isothermal annealing is consistent with the previous studies [8,10].

A very interesting observation of the microstructure evolution is that there is little intermixing of the

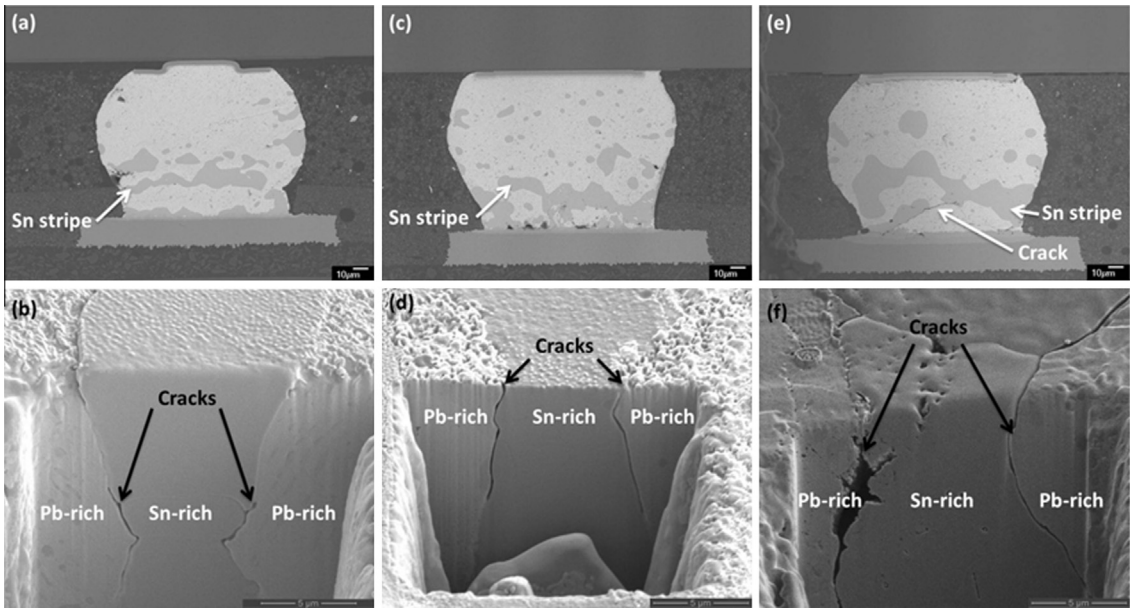

Figure 2. Cross-sectional SEM image and SEM image showing the FIB-polished second cross-section of the solder bump after TCT for (a and b) 500 cycles, (c and d) 1500 cycles, and (e and f) 14,410 cycles.

high-Pb phase and the eutectic SnPb phase in both isothermal and cycling annealing. This is because in a binary eutectic phase diagram such as SnPb, below the eutectic temperature, a constant temperature line is a tie-line of constant chemical potential. The phases along the tie-line, including the two primary phases at the ends of the two-phase region, are at equilibrium. This means there is no driving force or chemical potential gradient for compositional intermixing. In cycling annealing, there is a temperature change, and in turn a potential change. However, as long as the temperature change is uniform across the entire sample, or as long as there is no temperature gradient in the sample for any short period of time, the tie-line concept holds. The thickening of the Sn-rich and the Pb-rich phases can be due to ripening which reduces the total surface area or energy. Ripening can explain the growth of circular Sn grains, but it cannot explain the formation of the anisotropic Sn stripes. Furthermore, the formation of IMC via interfacial reactions with the Ni UBM and Cu bond-pad cannot explain the Sn stripe formation too. Therefore, we are left with the only driving force coming from the thermal stress potential gradient in cyclic annealing. This explains the formation of the Sn stripes and the crack formation along the Sn–Pb interfaces, to be discussed below.

Three-dimensional (3-D) finite-element analysis was employed in order to simulate the distributions of strain and stress in the composite solder joints in TCT. The model included the Si chip, the Ni UBMs, the solder joints, the Cu pads, the organic substrate and the underfill, as demonstrated in Figure 1a. In the simulation, the solder joint was composed of the spherical Sn5Pb95 solder bump above and the cup-like structure of the eutectic Sn63Pb37 solder beneath. The dimensions of the model were identical to those in the real flip-chip samples.

The distributions of strain and stress in the Sn5Pb95 solder are different from those in the Sn63Pb37 eutectic solder. Figure 3a depicts a 3-D simulation of the total mechanical and thermal equivalent strain distribution in the solder bump after one cycle of TCT. It is obvious that the Sn63Pb37 eutectic solder endured most of the strain, and the maximum tensile strain position in the eutectic solder is indicated by the arrow, as shown in Figure 3b. The simulation results of maximum strain position agree well with the experimental results that the crack formation was observed to initiate at the interfaces between the Sn-rich phase and the Pb-rich phase. Figure 3c and d illustrate the 3-D simulation of the hydrostatic stress distribution in the solder bump at

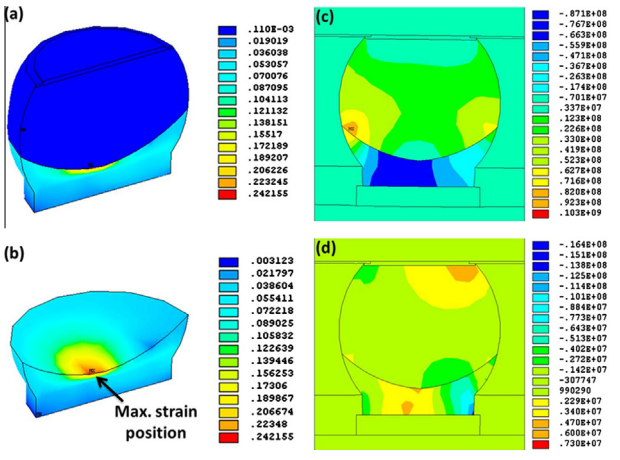

Figure 3. Simulation results for the total mechanical and thermal equivalent strain distribution in (a) the solder bump and (b) the Sn37Pb presolder after one cycle of TCT. And simulation results for the hydrostatic stress distribution in the solder bump at (c) −55 °C and (d) 125 °C.

the extreme temperatures, −55 and 125 °C, respectively. The scale bars are shown beside the figures. The positive values in the scale bars represent the tensile stresses, while the negative values indicate the compressive stresses. It can be observed that a tensile stress existed in the Sn5Pb95 on the chip side, whereas a compressive stress existed in the Sn63Pb37 eutectic on the substrate side. During TCT, the compressive stress region became larger when the ambient temperature was lower.

Under an elastic stress, microstructure evolution may occur to relieve the stress by creep, provided that atomic diffusion driven by the stress potential gradient can take place. Since Sn has a low melting point (505 K) and since the upper temperature of 125 °C (398 K) in the cycling tests is far above 0.5 of the melting point in absolute temperature, creep can occur. For the anisotropic growth of Sn grains in the horizontal or lateral direction, we need the stress-potential gradient in the vertical direction.

According to the Nabarro–Herring model of creep, atomic flux will diffuse from the compressive region to the tensile region. In Figure 3c and d, it is shown that the high-Pb is under tension and the eutectic is under compression, and we expect Sn atoms to diffuse from the eutectic to the necking region. Then the stress gradient in the necking region, as shown in Figure 3c and d, will induce a vertical diffusion of Sn from the high compressive stress region in the bottom of the joint to the necking region. This explains the anisotropic growth of the Sn stripe in the interfacial region between the high-Pb and the eutectic under TCT. In addition, the diffusivity of Sn and Pb were 7.77×10^{-29} and $1.64 \times 10^{-29}\ m^2\ s^{-1}$ at −55 °C, and 4.16×10^{-18} and $1.13 \times 10^{-18}\ m^2\ s^{-1}$ at 125 °C, respectively. It is obvious that the stress-migration flux of Sn is larger when the ambient temperature is higher due to the higher atomic diffusivity [20].

Generally speaking, cracks do not form along the lamellar interfaces in eutectic structure, especially in eutectic SnPb solder, which has been widely used for a very long time. It is a unique finding here that a crack forms in composite SnPb solder joints under TCT. Cracks tend to form under tension, not under compression. Indeed there is a tensile component in the stress distribution in the composite solder joint as shown in Figure 3c and d. Furthermore, the thicker the Sn phase, the larger the thermal strain due to the difference in thermal expansion coefficient between Sn and Pb. However, in TCT, we need to consider the fatigue contribution to the residual stress in crack formation in the composite solder joint. There must be a significant contribution from plastic deformation in the crack formation and propagation. The analysis of plastic contribution is beyond the scope of this paper. To do so experimentally, a change of the cyclic period to affect the creep process, which in turn affects the residual stress and strain, will be informative. More simulation work will clearly be needed.

The evolution of eutectic structure under isothermal and temperature cycle annealing has been studied. When the SnPb composite solder joints were subjected to a TCT between −55 and 125 °C, after 500 cycles the Sn grains coarsened and formed anisotropic Sn stripes near the necking site in the solder joint due to stress migration. Then the cracks, caused by the thermal stress, propagated along the Sn–Pb interfaces. After a prolonged 14,410 cycles of TCT, the Sn stripes penetrated almost the entire solder joint, and the cracks expanded accordingly. The 3-D simulation of the strain distribution supports the contention that the crack formation started at the Sn–Pb interfaces. Furthermore, instead of Sn stripes, only coarsened circular Sn grains were observed in the solder joints after a pure isothermal annealing at 150 °C. Therefore, stress migration of the Sn-rich phase triggered by the TCTs is a critical reliability issue in SnPb composite solder joints.

The financial support from the National Science Council, Taiwan, under the contract NSC 98-2221-E-009-036-MY3, is acknowledged.

[1] C.S. Chang, A. Oscilowski, R.C. Bracken, IEEE Circuits Device Mag. 14 (1998) 45.
[2] P.A. Totta, R.P. Sopher, IBMJ Res. Dev. 13 (1969) 226.
[3] L.F. Miller, IBMJ Res. Dev. 13 (1969) 239.
[4] D.O. Powell, A.K. Trivedi, in: Proc. 43rd Electron. Compon. Technol. Conf., IEEE, New York, 1993, pp. 182.
[5] R.K. Doot, in: Proc. 46th Electron. Compon. Technol. Conf., IEEE, New York, 1996, pp. 535.
[6] J.H. Lau, Ball Grid Array Technology, McGraw-Hill, New York, 1995.
[7] K.N. Tu, K. Zeng, Mater. Sci. Eng. R 34 (2001) 1.
[8] L.Y. Hung, P.H. Chang, C.C. Chang, Y.P. Wang, C.S. Hsiao, C.R. Kao, in: Proc. 3rd Int. Microsyst. Packag. Assem. Circuits Technol. IEEE, New York, 2008, pp. 255.
[9] C.C. Chang, Y.W. Lin, Y.S. Lai, C.R. Kao, J. Electron. Mater. 38 (11) (2009) 2234.
[10] C.C. Chang, Y.W. Wang, Y.S. Lai, C.R. Kao, J. Electron. Mater. 39 (8) (2010) 1289.
[11] C.L. Lai, C.H. Lin, C. Chen, J. Mater. Res. 19 (2) (2004) 550.
[12] A.T. Huang, A.M. Gusak, K.N. Tu, Y.S. Lai, Appl. Phys. Lett. 88 (2006) 141911.
[13] E.T. Ogawa, J.W. McPherson, J.A. Rosal, K.J. Dickerson, T.C. Chiu, L.Y. Tsung, M.K. Jain, T.D. Bonifield, J.C. Ondrusek, W.R. McKee, in: Proc. 40th Annu. Int. Reliab. Phys. Symp. IEEE, New York, 2002, pp. 312.
[14] T.C. Wang, T.E. Hsieh, M.T. Wang, D.S. Su, C.H. Chang, Y.L. Wang, J.Y.M. Lee, J. Electrochem. Soc. 152 (1) (2005) G45.
[15] H. Tsuchikawa, Y. Mizushima, T. Nakamura, T. Suzuki, H. Nakajima, Jpn. J. Appl. Phys. 45 (2A) (2006) 714.
[16] T.H. Chuang, H.J. Lin, C.C. Chi, Scripta Mater. 56 (2007) 45.
[17] T.C. Chiu, K.L. Lin, Scripta Mater. 60 (2009) 1121.
[18] Y. Sun, E.N. Hoffman, P.S. Lam, X. Li, Scripta Mater. 65 (2011) 388.
[19] K. Suganuma, A. Baated, K.S. Kim, K. Hamasaki, N. Nemoto, T. Nakagawa, T. Yamada, Acta Mater. 59 (2011) 7255.
[20] D. Gupta, K. Vieregge, W. Gust, Acta Mater. 47 (1) (1999) 5.